FC-BASED SEGMENTATION OF JAW TISSUES

Roberto Lloréns, Valery Naranjo, Miriam Clemente, Mariano Alcañiz and Salvador Albalat*

Instituto Interuniversitario de Investigación en Bioingeniería y Tecnología Orientada al Ser Humano
Universidad Politécnica de Valencia
Camino de Vera s/n, 46022 Valencia, Spain

Keywords: Jaw tissues segmentation, Dental implantology, Fuzzy connectedness, Mathematical morphology.

Abstract: The success of an oral implant surgery is subject to accurate advance planning. For this purpose, it is fundamental that a computer-guided program provides all the available information in a reliable way. Therefore, to plan a suitable implant placement, an accurate segmentation of the tissues of the jaw is necessary. These tissues are the cortical bone, trabecular core and the mandibular canal. The accurate segmentation of the mandibular canal, along which the inferior alveolar nerve crosses the lower arch, is particularly important since an injury to the canal can result in lip numbness. To this date, existing segmentation methods for the jaw requires high human interaction and/or don't achieve enough accuracy. Our overall aim is to develop an automatic method for the segmentation of the whole jaw, focusing our efforts on achieving very high accuracy and time efficiency. To this end, this paper presents an exhaustive evaluation of fuzzy connectedness object extraction as a plausible segmentation core for this method, basing on the results achieved on 80 CT slices in terms of detection and false alarm probability and merit factor.

1 INTRODUCTION

Dental implants are artificial roots, usually titanium-made, that are inserted into the maxillary bone in order to substitute the roots of the lost dental pieces, providing better functionality and aesthetics. For a long-term use, the placement of the implant must be inferred precisely and therefore the biometric properties of the patient's jaw must be known a priori. The lower jaw is the densest and most prominent bone of the face, and it is made up by three easily distinguishable tissues: a hard exterior cortical bone that contains a softer osseous tissue filling its inner cavity, the trabecular (or cancellous or spongy) bone, and the mandibular canal (when present), which contains the inferior alveolar nerve. This nerve runs along the lower jaw, from the mandibular to the mental foramen, supplying sensation to the teeth. For this reason, an injury to the canal might result in temporary or permanent lip numbness. All this gives rise to the need for an accurate segmentation which provides precise information to preoperative planning systems to assure the success of the dental surgery. Previous works

in segmentation of dental tissues require high human interaction and/or don't achieve enough accuracy to consider these approaches suitable for preoperative planning systems. Our research, then, is based on developing a method which provides this segmentation in an automatic and precise way.

The classical approach tries to plan the surgery from panoramic X-ray views, but this resource has a limited value due to the fact that it is an often-distorted two-dimensional image. CT is the more suitable evaluation method presenting 94% accuracy, whereas the periapical X-ray and the panoramic images present 53% and 17% accuracy, respectively (Reiser et al., 2004).

Many dental implant planning applications carry out the process of 3D reconstruction from CT data de-emphasizing tissue segmentation as in (Verstreken et al., 1998), and many others delegate this task to dentists or surgeons, providing tools with this purpose (Galanis et al., 2007). (Fütterling et al., 1998) carry out a segmentation of hard tissues by thresholding in strict sense while inner tissues are segmented by assigning different material properties to the tetrahedral finite elements, depending on the density gray values in the CT data-set. Obviously, any type of precision in the geometric model can therefore be omit-

409

ted. (W. Stein and Muhling, 1998) use Dijkstra's algorithm aided by 3D morphology to trace the most favorable path between two nodes (here, the mandibular and mental foramen) marked by an expert. (Kršek et al., 2007) present a tissue segmentation process which requires high human interaction assisted only by basic morphological operations and threshold in Hounsfield values. (Kang et al., 2007) use a fuzzy C-means-based partition tree for segmenting tissues with overlapped gray level range. (DeBruijne et al., 2003) adapted active shape models (ASM) to tubular structures. ASM are landmark-based linear shape models which try to fit a structure according to the variation represented in a training set previously annotated by an expert. (Rueda et al., 2006) follow this study and use active appearance models (AAM) for the segmentation of jaw tissues. However, since homologous points can not be established among different slices and some structures are unconnected or do not even appear, the precision achieved is completely insufficient.

Udupa et al. (Udupa and Samarasekera, 1996) present a novel method based on fuzzy subset theory with excellent results in different fields of medical imaging. In (Saha et al., 2000), several functions are proposed to represent intensity and homogeneity components of affinity. Our efforts are focused on evaluating all the configurations and validating them for the segmentation of jaw tissues in slices like those shown in figure 1, in order to create a complete automated 3D reconstruction valid for any preoperative dental implant planning system.

2 METHOD

Fuzzy connectedness (FC) has proven to give successful results in several medical applications such as multiple sclerosis lesion detection, blood vessel definition (Udupa et al., 1997a) and tissues segmentation (Udupa et al., 1997b). Our aim is to evaluate FC object segmentation in dental CT slices, defined transversally to the dental arch by means of a preoperative implant planning system, as shown in figure 1.

2.1 Theory Fundamentals

Fuzzy connectedness is a fuzzy subsets theory-based methodology. The algorithm starts from a *seed* and evaluates the affinity in a neighborhood of the pixels present in a queue. The queue is updated while the affinity is still able to be refined. In this way, the algorithm computes the *connectivity map* of the image under study, where each pixel value represents the
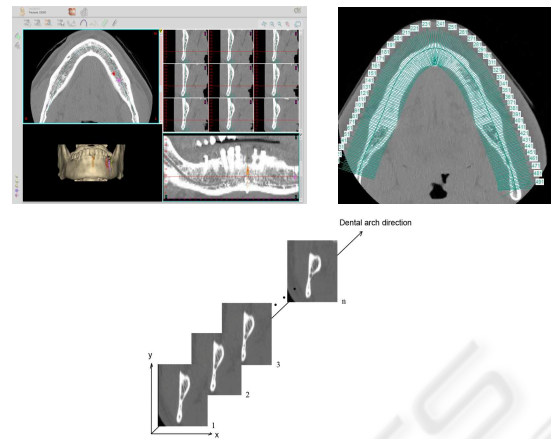

Figure 1: Definition of transversal slices by means of a planning system.

affinity between the pixel and the seed. Consequently, it is intuitive to define an object as those pixels whose connectivity value is greater than a threshold.

The affinity describes the similarity between two pixels and represents the power of the connection between them. For this reason the affinity is based on the adjacency between the pixels and on the similarity of their intensities. Adjacency represents the contiguity between pixels. For this study, 4-adjacency is considered and can be defined, for the pixels c_i and d_i, as follows:

$$\mu_\alpha(c,d) = \begin{cases} 1 & \text{,if } \sqrt{\sum_i (c_i - d_i)^2} \leq 1 \\ 0 & \text{,otherwise} \end{cases} \quad (1)$$
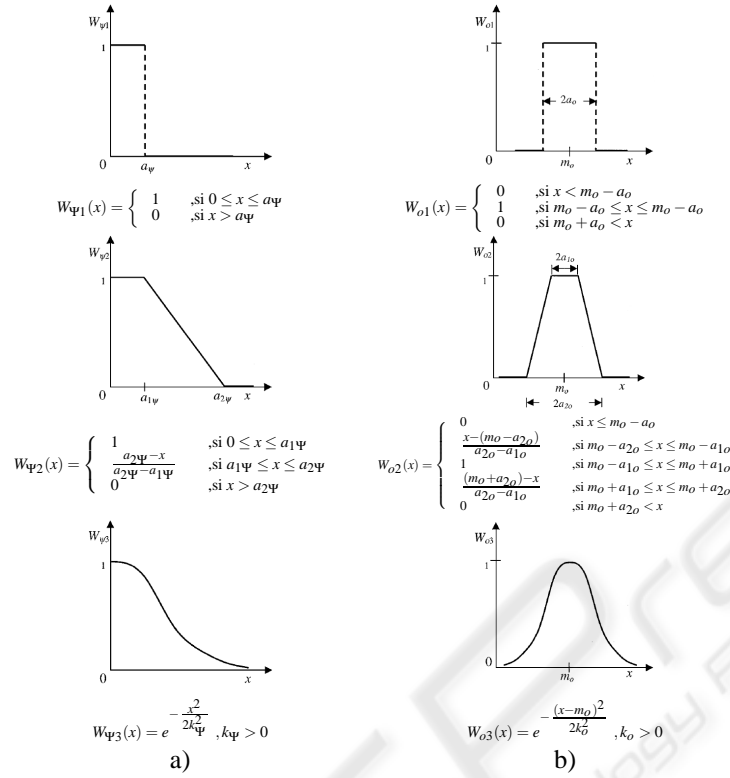
Analytically, the affinity can be expressed as:

$$\mu_\kappa(c,d) = h(\mu_\alpha(c,d), f(c), f(d), c, d) \quad (2)$$

That is, the affinity between the pixels depends on their adjacency, position and some function of them. According to the fuzzy connectedness theory described in (Saha et al., 2000), the affinity should consist of two components: an *object-feature-based component* and a *homogeneity-based component*. Both components must be considered in the design of the affinity, although in some applications it is more productive to consider only one component.

Therefore we can design a great variety of functions for each component independently and combine them to obtain the desired affinity relation valid for the application under study. Then, it is possible to refine the affinity as follows

$$\mu_\kappa(c,d) = \mu_\alpha(c,d)g(\mu_\Psi(c,d), \mu_\Phi(c,d)) \quad (3)$$

where μ_Ψ and μ_Φ represent the homogeneity-based and the object-feature-based component, respectively. The strength of relation Ψ represents the degree of the

$$W_{\Psi 1}(x) = \begin{cases} 1 & ,si\ 0 \le x \le a_\Psi \\ 0 & ,si\ x > a_\Psi \end{cases}$$

$$W_{o1}(x) = \begin{cases} 0 & ,si\ x < m_o - a_o \\ 1 & ,si\ m_o - a_o \le x \le m_o - a_o \\ 0 & ,si\ m_o + a_o < x \end{cases}$$

$$W_{\Psi 2}(x) = \begin{cases} 1 & ,si\ 0 \le x \le a_{1\Psi} \\ \dfrac{a_{2\Psi}-x}{a_{2\Psi}-a_{1\Psi}} & ,si\ a_{1\Psi} \le x \le a_{2\Psi} \\ 0 & ,si\ x > a_{2\Psi} \end{cases}$$

$$W_{o2}(x) = \begin{cases} 0 & ,si\ x \le m_o - a_o \\ \dfrac{x-(m_o-a_{2o})}{a_{2o}-a_{1o}} & ,si\ m_o - a_{2o} \le x \le m_o - a_{1o} \\ 1 & ,si\ m_o - a_{1o} \le x \le m_o + a_{1o} \\ \dfrac{(m_o+a_{2o})-x}{a_{2o}-a_{1o}} & ,si\ m_o + a_{1o} \le x \le m_o + a_{2o} \\ 0 & ,si\ m_o + a_{2o} < x \end{cases}$$

$$W_{\Psi 3}(x) = e^{-\frac{x^2}{2k_\Psi^2}}, k_\Psi > 0$$

$$W_{o3}(x) = e^{-\frac{(x-m_o)^2}{2k_o^2}}, k_o > 0$$

a) b)

Figure 2: Expressions of μ_Ψ (column a) and μ_Φ (column b) considered.

union of the pixels due to the similarity of their intensity levels. The strength of relation Φ represents the degree of the union due to the similarity of some specific characteristic.

So, every function which combines these two affinity components, satisfying the theoretical restrictions described in (Saha et al., 2000), is a valid expression of g. The set of functions evaluated in the presented study was:

$$\mu_\kappa = \mu_\alpha \sqrt{\mu_\Psi \mu_\Phi} \qquad (4)$$

$$\mu_\kappa = \mu_\alpha (\omega_1 \mu_\Psi + \omega_2 \mu_\Phi) \qquad (5)$$

$$\mu_\kappa = \mu_\alpha ((1 - \min(\mu_\Psi, \tfrac{1}{2}\mu_\Phi))\mu_\Phi + \min(\mu_\Psi, \tfrac{1}{2}\mu_\Phi)\mu_\Psi) \qquad (6)$$

2.1.1 Homogeneity-based Component

The homogeneity-based component between two pixels c and d can be modeled by $|f(c) - f(d)|$, which indeed represents their unhomogeneity , and consequently μ_Ψ can be expressed as a function of that difference.

$$\mu_\Psi(c,d) = W_\Psi(|f(c) - f(d)|) \qquad (7)$$

The evaluated functions, extracted from the fuzzy subsets theory, are shown in figure 2, where $x = |f(c) - f(d)|$ in all the cases.

2.1.2 Object-feature-based Component

The feature considered is the intensity of the pixels. The functions for modeling this component are the homologous of the homogeneity-based case, and are shown in figure 2, where $x = \frac{f(c)+f(d)}{2}$ for this component description.

2.2 Segmentation Process

The complete segmentation of the jaw is carried out, as shown in figure 3, applying FC on the cortical bone (upper branch) and the mandibular canal (lower branch). The trabecular core is obtained as the inner zone of the cortical which is not considered canal.

As a result of this definition, the cortical bone must be a closed structure, hence a morphological processing is implemented to add the boundary to the cortical. This process is shown in figure 4.

For the cortical processing, the seed is selected as the pixel with maximum value in the distance matrix, which is extracted from a previous coarse estimation of the cortical.

The initial estimation of the cortical bone is obtained by thresholding the *region of interest* (ROI),
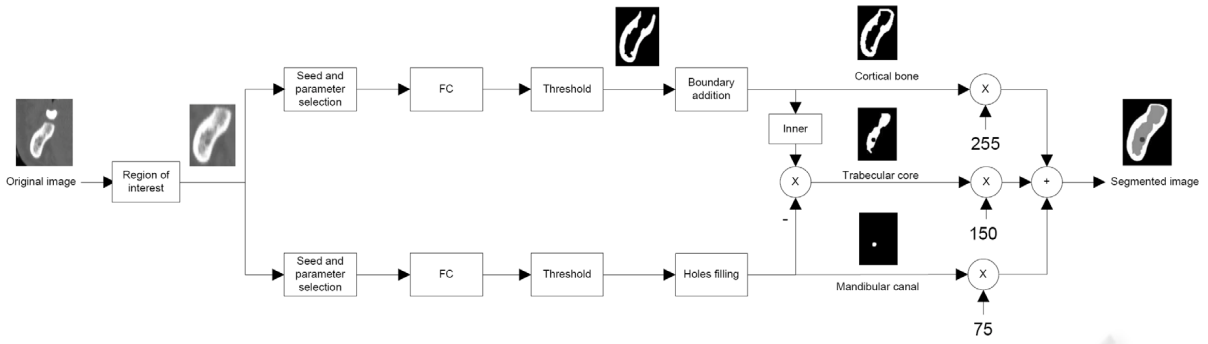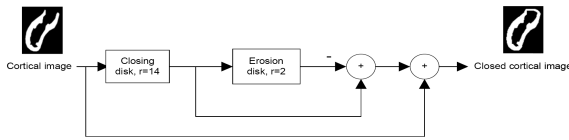
Figure 3: Segmentation process diagram.

Figure 4: Boundary addition diagram.

since it takes values saturated to 255, and is also used to estimate the parameters needed for the FC segmentation. For the canal processing, the seed is manually selected and the parameters are estimated in a neighborhood of it.

3 RESULTS

Defining g, μ_Ψ and μ_Φ it is possible to generate an affinity family, for any given fuzzy relation κ, μ_κ. Our aim is to evaluate all the possible configurations ζ_{lmn} to find the combination with the best performance for the segmentation of jaw tissues.

$l, m, n \in [1, 2, 3]$ refer respectively to the three possible g, μ_Ψ and μ_Φ considered in section 2.1. The parameters used to define these components were

μ_Ψ	$a_\Psi = M_h + t\sigma_h$, $a_{1\Psi} = 0$, $a_{2\Psi} = M_h + t\sigma_h$, $k_\Psi = M_h + t\sigma_h$
μ_Φ	$m_o = M_o$, $a_o = t\sigma_o$, $a_{1o} = 0$, $a_{2o} = t\sigma_o$, $k_o = t\sigma_o$

where (M_o, σ_o) and (M_h, σ_h) are the mean and the standard deviation of the intensities and the intensity differences (respectively) of the defined cortical and channel regions.

In all the cases, the results have been evaluated by comparing the segmentation obtained with the *groundtruth set*, consisting of 80 CT slices manually segmented by a group of 5 experts. The resulting images have been evaluated using the *detection* and *false alarm probability* and the *merit factor* defined as follows:

$$DP = \frac{count(im_{seg} \text{ AND } im_{gt})}{count(im_{gt})} \quad (8)$$

$$FAP = \frac{count(im_{seg} \text{ AND } \overline{im_{gt}})}{count(im_{gt})} \quad (9)$$

$$MF = max(1 - \frac{count(im_{seg} \text{ XOR } im_{gt})}{numpixels}) \quad (10)$$

, where im_{seg} refers to the segmented image, and im_{gt} and $\overline{im_{gt}}$ refer to the groundtruth and inverted groundtruth images, respectively. The process followed can be summarized in fixing a possible function g, and evaluating all combinations of μ_Ψ and μ_Φ. The configurations with the best performance and their respective merit factors are shown in table 1. It can be deduced that the best configuration is ζ_{323}, for both the cortical and channel tissues.

Table 1: Best configurations comparison.

Combination function g	Best configuration	Cortical bone	Mandibular canal
eq 4	ζ_{123}	96.185	99.717
eq 5	ζ_{231}	96.852	99.240
eq 6	ζ_{323}	96.962	99.739

Likewise, figure 5 shows the detection and false alarm probability vs the threshold level used for binarizing the connectivity map for the cortical bone and mandibular canal. Finally, figure 6 shows the results obtained when the proposed segmentation process was applied to some test set slices. The algorithm processing time is approximately 1 second per image of 153×180 pixel (using MATLAB on a Pentium IV at 2.8 GHz and 1 GB of RAM).

4 DISCUSSION

In this paper a new segmentation method for dental CT slices based on FC object extraction theory and mathematical morphology has been presented. For this purpose, all the possible combinations of the
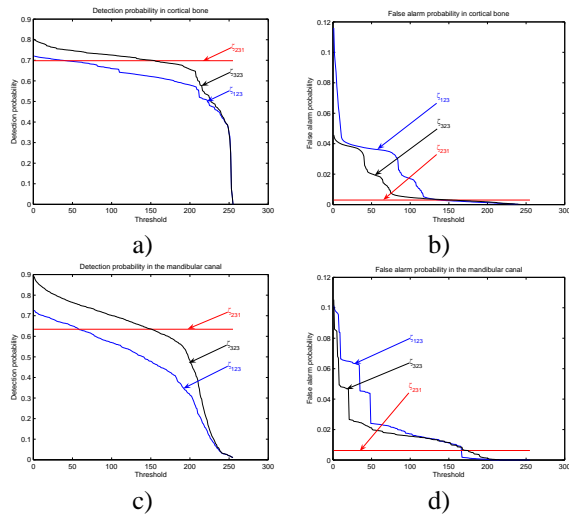
Figure 5: a) and b): Detection and false alarm probability in the cortical bone. c) and d): Detection and false alarm probability in the mandibular canal.

functions under study have been exhaustively evaluated and the best configuration has been used for segmenting the tissues of the jaw in 80 dental CT slices, achieving great accuracy in both cortical and canal cases with merit factors of 96.962 and 99.739, respectively. The trabecular core was also successfully obtained as the inside of the cortical which is not considered canal. Furthermore, the presented method has a very low computational cost, which makes it suitable for our overall purpose of segmenting and reconstructing the whole jaw. Future research will focus on adapting the presented method to this end and on dynamically adjusting the FC parameters to each slice processed.

REFERENCES

DeBruijne, M., Ginneken, B. V., Viergever, M. A., and Niessen, W. (2003). Adapting active shape models for 3d segmentation of tubular structures in medical images. In *Information Processing in Medical Imaging*. Springer.

Fütterling, S., Klein, R., Straer, W., and Weber, H. (1998). Automated finite element modeling of a human mandible with dental implants.

Galanis, C. C., Sfantsikopoulos, M. M., Koidis, P. T., Kafantaris, N. M., and Mpikos, P. G. (2007). Computer methods for automating preoperative dental implant planning: Implant positioning and size assignment. *Computer Methods and Programs in Biomedicine*, 86(1):30–38.

Kang, H., Pinti, A., Vermeiren, L., Taleb-Ahmed, A., and Zeng, X. (2007). An automatic fcm-based method for
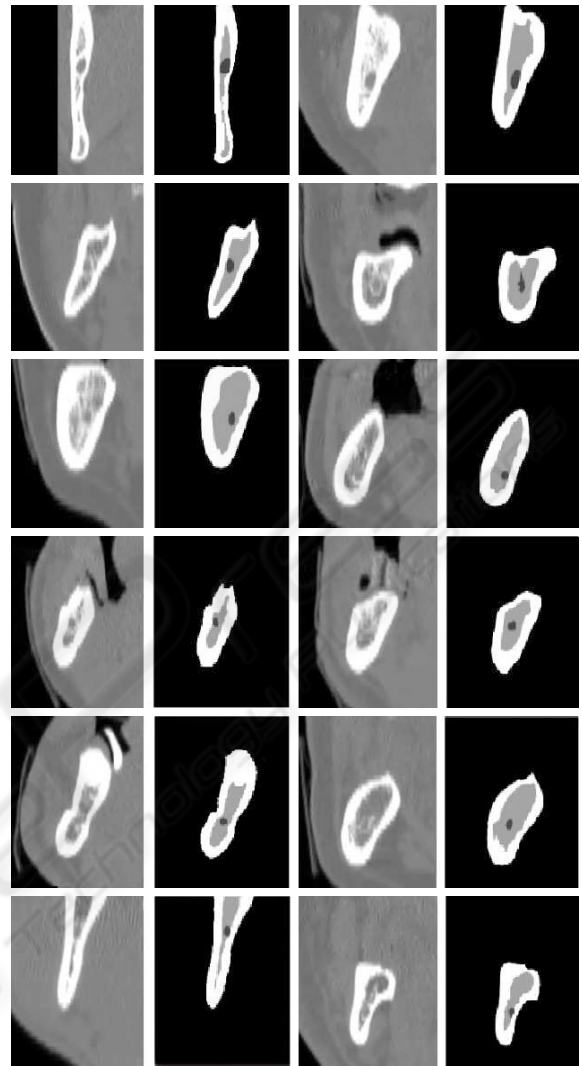
Figure 6: Results obtained with the proposed method.

tissue classification. In *The 1st International Conference on Bioinformatics and Biomedical Engineering*, pages 510–514. IEEE Computer Society.

Kršek, P., Krupa, P., and Cernochov, P. (2007). Teeth and jaw 3d reconstruction in stomatology. In *Medical Information Visualisation - BioMedical Visualisation*. IEEE Computer Society.

Reiser, G. M., Manwaring, J. D., and Damoulis, P. D. (2004). Clinical significance of the structural integrity of the superior aspect of the mandibular canal. *Journal of Periodontology*, 75(2):322–326.

Rueda, S., Gil, J. A., Pichery, R., and niz, M. A. (2006). Automatic segmentation of jaw tissues in ct using active appearance models and semi-automatic landmarking. In *Medical Image Computing and Computer-Assisted Intervention MICCAI 2006*. Springer.

Saha, P. K., Udupa, J. K., and Odhner, D. (2000). Scale-based fuzzy connected image segmentation: Theory,

algorithms, and validation. *Computer Vision and Image Understanding*, 77(2):145–174.

Udupa, J. and Samarasekera, S. (1996). Fuzzy connectedness and object definition: Theory, algorithms, and applications in image segmentation. *Graphical Models and Image Processing*, 58(3):246–261.

Udupa, J. K., Odhner, D., Tian, J., Holland, G., and Axel, L. (1997a). Automatic clutter-free volume rendering for mr angiography using fuzzy connectedness. *In SPIE Proceedings Medical Imaging*, 3034:111119.

Udupa, J. K., Tian, J., Hemmy, D., and Tessier, P. (1997b). A pentium pc-based craniofacial 3d imaging and analysis system. *J. Craniofacial Surgery*, 3031(138):333339.

Verstreken, K., Cleynenbreugel, J. V., Martens, K., Marchal, G., van Steenberghe, D., and Suetens, P. (1998). An image-guided planning system for endosseous oral implants. *IEEE Transactions on Medical Imaging*, 17(5):842–852.

W. Stein, S. H. and Muhling, J. (1998). Tracing of thin tubular structures in computer tomographic data. *Computer Aided Surgery*, 3(2):83–88.